Journal of Electronics and Electrical Engineering
https://ojs.wiserpub.com/index.php/JEEE

Research Article

Investigation into Shaped Wide-Beam Reflectarray Surfaces Reflectors as Passive Repeaters in Wireless Networks

Peter Callaghan*, Paul R. Young

School of Engineering, University of Kent, Canterbury, UK
E-mail: pc395@kent.ac.uk

Received: 17 October 2024; **Revised:** 11 December 2024; **Accepted:** 3 January 2025

Abstract: This paper investigates the use of a Reflectarray Surface (RAS) to provide a shaped beam for use as a passive repeater in a wireless network. A shaped beam can be desirable as it may provide coverage over a dead-spot region. Examples of a flat-topped and sloping top shaped beams having a nominal beamwidth of 30° and a steering angle of 40° at 10 GHz are investigated, designed using the particle swarm optimizer in MATLAB. Measurement and simulation from CST show reasonable agreement to the 'array factor' synthesis patterns but display practical detuning effects that may limit this approach. Additionally, it was noted element factor has a more significant impact on such beam shaping.

***Keywords*:** reflectarrays, metasurfaces, passive repeater, beam steering, reconfigurable intelligent surfaces

1. Introduction

Reflectarray surfaces reflectors (RSR), also called metasurfaces, formed from a doubly periodic array of reflecting elements can cause non-specular scattering of electromagnetic waves. Such surfaces have been used successfully in replacing curved reflectors in large antennas [1]. In recent years RSR have received renewed interest for use as passive repeaters in wireless networks [2, 3, 4, 5, 6, 7, 8, 9]. Such networks can suffer from 'dead-spots' as illustrated in Figure 1a. Here the direct path from a base station or access point to a user is masked by an obstacle that reduces the signal level significantly. Here a RSR sited behind the user can re-direct sufficient energy to maintain connectivity. Examples of such RSR are becoming available [10, 11] for use in 5G wireless networks. In wireless mobile application the position of the user can change and therefore the beam angle needs to be adjustable. This is possible using electronic means [12] creating a Reconfigurable Intelligent Surface (RIS), so-called as they can offer additional advantages when integrated with the communications system [13]. Much work is currently looking at practical realization of RIS [14]. To reflect adequate energy the RAS needs to be electrically large usually resulting in a pencil beam having a narrow width, as indicated in Figure 1a. Obviously for a general application the position of the user can change and therefore the beam angle needs to be adjustable. This may be achieved by various methods, such as mechanically [9] or electronically [10].

Virtually all the RSR and RIS considered to date have one common limitation in that they produce a 'pencil-beam' (see inset in Figure 1a). However, it has been argued for more practical systems RIS and RASR should use shaped beams. A pencil beam may not provide sufficient pointing accuracy or a large enough coverage area [15]. It is also noted that RAS can exhibit 'frequency-scanning' effects that limit the frequency bandwidth that can be compensated by using beam

DOI: https://doi.org/10.37256/jeee.4120255938

widening [16]. An alternative approach is to compensate the entire shadow region using a single shaped beam RSR as illustrated in Figure 1b. In [9] it was proposed that a minimum size for the RSR be defined to ensure the signal power in the shadow region is equivalent to that without the obstruction. Extending this principle here means that path length losses also need to be compensated, requiring a $1/\cos^2(\theta)$ shaped beam, as indicated by Figure 1b inset. The standard approach for creating a shaped beam pattern using arrays is by adjusting the element amplitudes using Fourier transform techniques [11]. For the RAS problem considered here the illumination is uniform with 100% reflection desired (to avoid loss of energy) so the only parameter that can be adjusted is the phase of individual elements. An integral equation can be set up that relates the antenna pattern to the element phases but this cannot be solved directly so an alternative approach is needed.

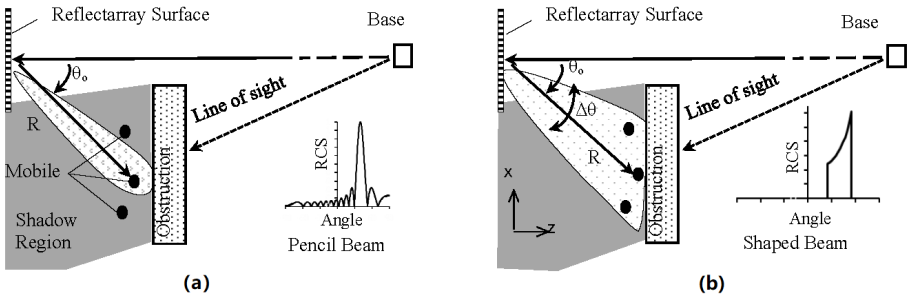

Figure 1. Passive repeater using a reflectarray surface to eliminate a dead-spot in wireless networks. (**a**) Conventional 'Linearly phased' RAS (**b**) RAS with beam shaping

The challenge is to define the element phases of the RSR that radiate a prescribed shaped beam as described by the array factor model [1]. Closed form expressions from [17], using a RSR to replace an elliptically profiled solid reflector, can give a flat-topped beam but there is limited control of the beamwidth. A more general approach is to use numerical methods to find the element phases. Such methods have already been applied in the design of shaped beam reflectarray antennas [1]. A local search method can be applied such as the alternating projector method used in [18] used to form flat topped and cosecant shaped beams and in [19] to form a multi-beam transmitarray. More recent approaches use a global search technique such as Particle Swarm Optimization (PSO). This approach has proved popular with examples of the PSO being used to create a flat topped beam of 30° width in azimuth but cosecant shaped in elevation [20, 21], null steering in a pencil beam reflectarray antenna [22] and even to design the element itself to achieve a dual band RSR [23]. In more recent years, the design of reflectarray antennas for space applications are using Machine Learning techniques to optimize the element parameters directly to give a desired pattern, controlling both co-polar and cross-polar levels [24, 25]. However reflectarray antenna shaped beams are typically flat-topped and at low angles (<30°). One design [21] did consider a $1/R^2$ shape but this decayed with increasing angle whilst for the dead spot problem of Figure 1b the power needs to increase.

Modern numerical techniques using 'AI' optimization techniques and 'digital twins' that model the RSR elements have recently been applied to the design of RSR [26] presenting design examples of complex multi-beam and focused beam patterns. However, [26] uses proprietary software for the design, again based on 'array factor' model, with confirmation using commercial electromagnetic software (HFSS). This paper investigates wider, shaped beam patterns to illuminate a dead-spot region as in Figure 1 such that mobile users retain coverage without the need of a complex RIS system. For this use is made of a commercially available PSO optimizer in MATLAB to design the element. Confirmation is made using the commercial electromagnetic software package CST microwave studio (CST MWS) but also experimentally.

2. Beam shaping using phase only

We have taken the approach of using PSO to find the element phases for a RAS to satisfy the problem in Figure 1b. We also assumed the reflected and the incident waves are in the same plane (xoz) such that there is no beam steering in the orthogonal planes. This is actually representative of many practical situations such as the 'corridor' problem [2, 5]. It is

also assumed the incident wave is far from the base such that it can be considered a plane wave normal to the surface. This simplifies the problem to finding the phases for a linear array. The beam shape is defined by the Array Factor (AF) Equation (1).

$$AF(\theta) = \frac{1}{N}\sum_{i=0}^{N-1} e^{j\psi_i} e^{jkx_i \sin(\theta)} \tag{1}$$

where x_i are the position of the individual elements defined by:

$$x_i = id - \frac{Nd}{2}, \quad i = 0, 1, 2 \ldots (N-1)$$

k is the wave number ($2\pi/\lambda$), d is the element spacing (periodicity), N are the number of elements and ψ_i are the phases generated by the PSO routine for beam shaping. The AF is normalized by $1/N$ whereby the energy is shared equally between the elements as the incident wave is assumed a plane wave. If the phases, $\psi_{Li,}$ have a linear phase shift as described by (2) a pencil beam in the direction θ_o is formed.

$$\psi_{Li} = -kx_i \sin(\theta_o) \tag{2}$$

For a shaped beam we define a *mask* function (3) that is used by the PSO to determine a set of phases to give a desired AF pattern. M_2 and M_3 define the AF beam levels at the beam edges θ_2 and θ_3, such that the nominal beam level $M_{23}(\theta)$ between angles $\theta_2 < \theta < \theta_3$ follows a straight line. ΔM defines the desired limit of any beam variation between M_2 and M_3 from this straight line. M_1 and M_4 define maximum sidelobe levels below θ_1 and above θ_4 respectively.

$$mask = \begin{cases} |AF| < M_1 & -90^\circ < \theta < \theta_1 \\ Max(\Delta AF) < \Delta M & \theta_2 < \theta < \theta_3 \\ |AF| < M_{23}(\theta) & \theta_2 < \theta < \theta_3 \\ |AF| < M_4 & \theta_4 < \theta < +90^\circ \end{cases} \tag{3}$$

where

$$Max(\Delta AF) = Max(AF) - Min(AF)$$

$$Max(\Delta AF) = Maximum(AF) - \left(M_{23}(\theta) - \frac{\Delta M}{2}\right)$$

$$Min(\Delta AF) = Min(AF) - \left(M_{23}(\theta) + \frac{\Delta M}{2}\right)$$

In practice an error value is calculated for portions of the AF that exceed the mask. The error term is calculated using an RMS value taken over the range of angles. Additionally, we allowed each section of the mask to have a weighting factor to allow the optimization routine to focus on in-beam or out of beam characteristics to facilitate finding a best solution. An algorithm was written in MATLAB using their in-built PSO function. Starting values for the PSO were taken using (2). The swarm size was varied to minimize computational time but to achieve a good solution. For the 20-element array considered in this work a swarm size of 180 was used. An outline of the algorithm used in the MATLAB m-file is presented in Algorithm 1.

Algorithm 1 Particle Swarm Optimization for Phase Fitting (Outline using MATLAB)

Input/define the following
N: number of elements
F: Frequency
d: Element spacing
$x(i)$: (vector) are the element positions along the x-axis (see (1))
phases: (vector) element phases ψ(i)—need to set initial values for PSO
$\theta(i)$: (vector) angles that array factor (AF) pattern calculated at (i.e., typically -90° to 90° step 1°)
lb = (vector) lower bound for phases (-360°)
ub = (vector) lower bound for phases (0°)
Mask defined by levels M = [M1 M2 M3 M4 ΔM], angles θ([θ1 θ2 θ3 θ4] and weights W([W1 W2 W3 W4]
%Define the following function
fun = @(phases) fit_phases(phases)
options = optimoptions('particleswarm', 'SwarmSize', 180, 'InitialSwarmMatrix', phases, 'ObjectiveLimit', $1e^{-8}$, 'FunctionTolerance', $1e^{-8}$, 'HybridFcn', @fmincon)
[phases, fitness, exitflag, output] = particleswarm(fun, N, lb, ub, options); % Invokes the PSO optimiser
function erf = fit_phases(ψ(i)), N, x(i), θ(i), θ(i), Mask)
calculate AF from (1) using F, ψ(i)), N, x(i), θ(i))
Then Calculate error function:
for $\theta = -90$ to θ_1 **do**
    if $AF > M_1$ **then**
        $Err_1 = Err_1 + AF^2$
    end if
end for
$Slope = \frac{M_3 - M_2}{\theta_3 - \theta_2}$
$Const = \frac{\theta_3 M_2 - \theta_2 M_3}{\theta_3 - \theta_2}$
for $\theta = \theta_3$ to θ_4 **do**
    $M_{nom} = Slope \cdot \theta + Const$
    $M_{max} = M_{nom} + \frac{\Delta M}{2}$
    $M_{min} = M_{nom} - \frac{\Delta M}{2}$
    if $M_{max} > RippleMax$ **then**
        $RippleMax = M_{max}$
    end if
    if $M_{min} < RippleMin$ **then**
        $RippleMin = M_{min}$
    end if
    if $AF < M_{nom}$ **then**
        $Err_2 = Err_2 + AF^2$
    end if
end for
$Err_3 = \sqrt{(M_{max} - M_{min})^2 - \Delta M^2}$
for $\theta = \theta_4$ to 90 **do**
    if $AF > M_4$ **then**
        $Err_4 = Err_4 + AF^2$
    end if
end for
$Erf = W_1 \cdot \sqrt{Err_1} + W_2 \cdot \sqrt{Err_2} + W_3 \cdot \sqrt{Err_3} + W_4 \cdot \sqrt{Err_4}$

3. Flat-topped shaped beam

For the problem in Figure 1b we consider an RAS of 20 × 20 elements with a period of 10 mm operating at 10 GHz to give a spread beam at θo = 40°, of width Δθ (=$\theta_2 - \theta_3$) = 30°. This size was chosen to suit the limitations of our experimental set-up (see Section 5). Initially we considered a flat-topped beam such that the radio energy is spread equally over the beam. For conservation of energy, the peak RCS will fall as the beamwidth widens, so we set the in-beam level to be −6 dB (relative to a linearly phased array) with a ripple of 0.5 dB. The sidelobes were to be below a level of −20 dB. Suitable values for the phases were calculated as shown in Figure 2. In Figure 2a the actual phases are plotted for a linear (from (2)) and an 'elliptical' (from [17]) function. The linear portion from (2) is 77° per element. This gives a total phase change of 1465° across the array. This masks the much smaller non-linear portion of the elliptical phases that cause the beam shaping, typically less than 200°. Therefore in Figure 2b. we plot the difference between the 'shaped' phases and that for a linearly phased beam (pencil beam). The resulting AF is plotted against the mask in Figure 3. For comparison the phases and the AF for an 'elliptically' phased array [17] have also been added to these figures. For this arrangement the 'Elliptical' phasing gives very similar results. The PSO gives closer agreement to the wanted ripple although has slightly higher sidelobes. As expected, the phases compare closely with the Elliptic, presenting a smooth curve (phases determined by an equation) whilst the PSO phases follow a similar shape but with some small variations, being based on choosing a random set of phases. This confirms the convergence of the PSO to be suitable for this problem.

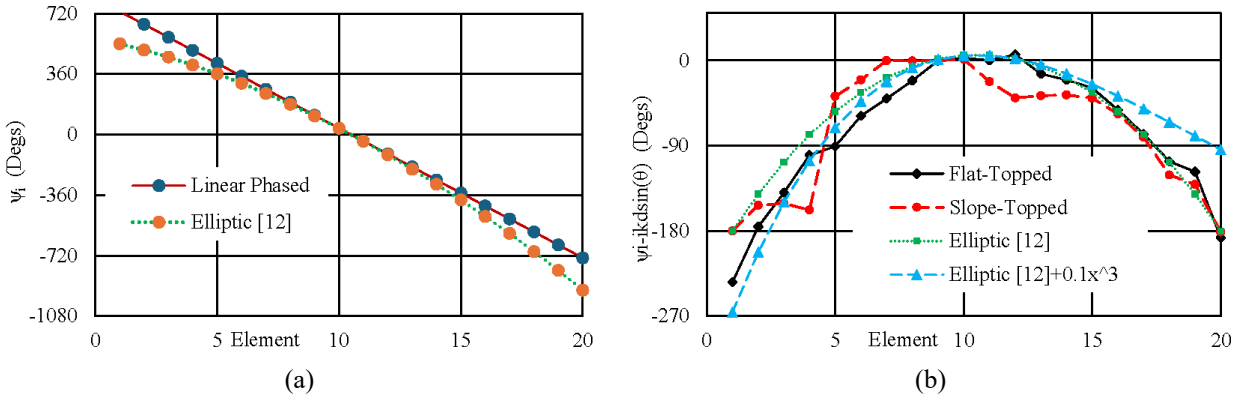

Figure 2. Element phases (**a**) Actual phases for linear and elliptic (**b**) 'difference' from 'linear' phasing (i.e., ψ_i-ikdsin(θ)) highlighting shaping

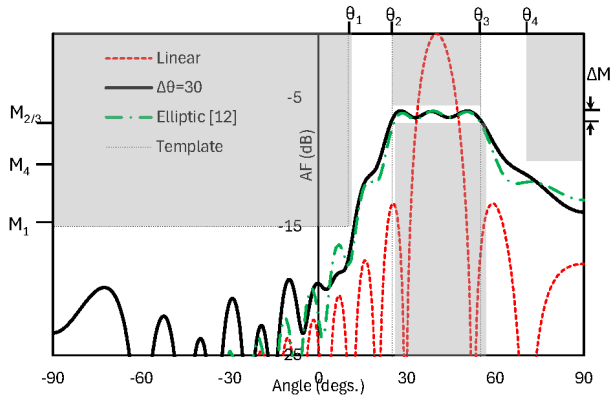

Figure 3. Flat topped beam from PSO compared to linear and 'Elliptic' phased elements. (P = 10 mm, N = 20, θ = 40°, Δθ = 30°)

The choice of beamwidth for this 20-element array at this frequency meant the Elliptical phases can meet this requirement but in general this is not the case, as the beamwidth for Elliptical phasing is determined by the aperture size.

The PSO, in principle, can be used to determine an arbitrarily defined beam (assuming a solution exists). To illustrate we next considered the problem of increasing the beam width to spread the energy further. As the beam is spread the peak RCS will fall further. This presents a problem for a practical application as field levels in the 'dead-spot' will need to meet a minimum level. However, the number of elements can be increased (i.e., increase the physical area) to compensate as given by (4).

$$N_2 = N_1 \frac{\Delta\theta_2}{\Delta\theta_1} \tag{4}$$

As an example, consider again our nominal design of θo = 40°, Δθ = 30° and N_1 = 20. To design an RAS with beamwidths of 20° and 40° we determine the number of elements from (4) to achieve the same RCS in the beam as the original RAS, listed in Table 1. (For comparison we also considered a linearly phased RAS.). The actual RCS can be calculated from (5) where M is the number of elements in the orthogonal direction, being 20 in our example. (Note EF is an 'element factor' assumed unity at this stage). Table 1 notes the maximum RCS of the shaped beam, $Max(RCS(\theta))$, and also the peak RCS, $RCS(\theta o)$, for a linearly phased pencil beam.

$$RCS(\theta) = 4\pi EF \left(\frac{NMd^2}{\lambda}\right)^2 AF(\theta) \tag{5}$$

Table 1. RCS-compensation for widening beam

Beamwidth	14°	20°	30°	40°
N	10	13	22	27
RCS(θo)	7.5	9.7	13.5	16.1
Max(RCS(θ))	7.5	6.4	7.5	8.0

The PSO routine was used again to find appropriate phases giving the bi-static RCS patterns in Figure 4. As can be seen the PSO routine successfully finds solutions to give wider and narrower beamwidths that have a similar RCS value in the beam. The linear beam of 10 elements is quite similar to the 13-element shaped beam—giving an illustration of the limits of this approach. In general, higher numbers of elements gives greater control but also a much larger number of possible solutions. The beam shaped for N = 27, Δθ = 40°, is not ideal—it may be possible that a better solution could be found (by increasing the swarm size, adjusting the weighting factors).

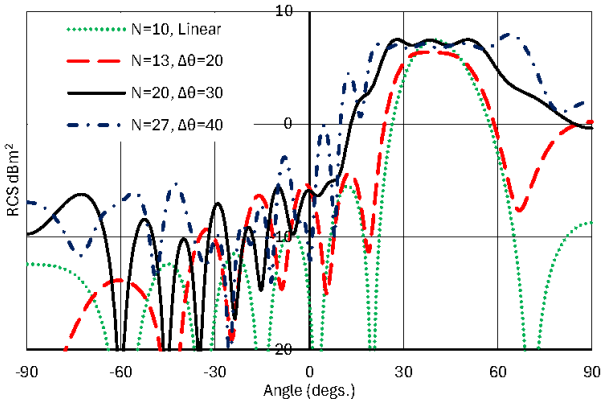

Figure 4. Bistatic RCS compensation of RCS by increasing array size for wider beamwidth. Array size is 20 × N. θ = 40°

4. Shaped beam to compensate for range variation

The flat-topped beam discussed in Section 3 will fill the 'dead-spot' problem of Figure 1b. However, if the beam width is relatively large, as Figure 1b suggests, then the change of range across the beam will impact the signal level at the receiver, placed behind the obstruction. It is desirable for the amplitude of the beam to increase at higher angles. Here we can use the PSO routine to generate a sloping shaped beam similar to that achieved in [15]. A difference here is that in [15] the amplitude falls with increasing angle.

The template for the beam was modified to compensate for the $1/R^2$ path losses with a linear change of 6 dB between the lower and higher edges of the beam (linear as in dB). The linear phase slope of (2) causes a shift in the beam direction so we explored the impact of adding a cubic term to the elliptic phase distribution of [17] to skew the flat-topped beam. Such a phase distribution has been added to Figure 2 with some success in achieving a sloping beam pattern in Figure 5a. However, this is far from ideal so the PSO is needed to optimise the shape. Using an elliptic phase distribution [12] for initial values the PSO took 551 iterations, reducing the fitness value from 6.12 to 0.012. Phases from the PSO plotted in Algorithm 1 show more subtle, but complex differences to the elliptic phase profile but achieved a pattern in close agreement to the design template.

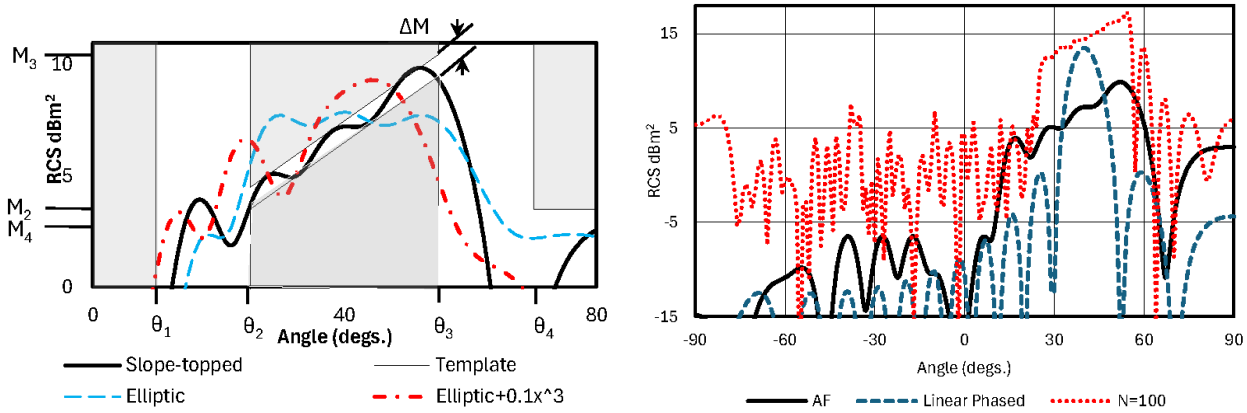

Figure 5. Bistatic RCS in XOZ plane for Ex illumination of array in Figure 6—elements optimized for a sloping shaped pattern ($\theta_o = 40°$, $\Delta\theta = 30°$) (**a**) main beam shape for N = 20 (**b**) comparison of N = 20 and N = 100 shaped beam to N = 20 linear (pencil) beam

The beam generated by the 'PSO' phases exhibits a sidelobe around 20° in the 'guard' region, which is ignored by the optimizer. In this instance this is beneficial as it extends the sloped beam. The sidelobes at wider angles are seen in Figure 5b to be typically 20 dB below the peak of a linearly phased RAS, also plotted for comparison. Here the energy loss caused by widening the beam is apparent. In practice, if this 20 element linearly phased RAS gave a suitable received signal level in the shadow region then from (4) a sloping beam RAS would need to have 100 elements, as suggested by other authors [15, 24]. A typical pattern for a PSO optimized 100 element sloped beam RAS has been added to Figure 4b. Not only does this show that the level has been compensated but for larger arrays the beam shape has a much greater definition.

5. Practical evaluation

Whilst the array factor predictions promise useful shaped beams in practice the pattern can be degraded by factors such as mutual coupling, element factor and losses. To investigate the impact of such factors two practical RAS were fabricated. The element design chosen was a stub loaded patch [20] as this offers a reasonably linear element tuning curve and minimizes mutual coupling. The practical design, presented in Figure 6, is a 20 × 20 element linearly polarized RAS, designed to operate at 10 GHz, with periodicity of 10 mm.

The dimensions were adjusted to make the phase versus stub length (=L1 + L2 + L3) relationship as linear as possible [20]. The element phase as a function of stub length was calculated using the Unit Cell tool in the frequency domain model of CST MWS and is plotted in Figure 7. This achieves a total phase change of nearly 540°. However, the element phase change across the array for 20 elements is around 1500°. As such phase wrapping is needed, limiting the phase change to 360° and using the first portion of the curve that is most linear, as indicate by the straight line. It is worth noting that many reflectarray antenna designs use lower incidence angles, or indeed a feed at oblique incidence resulting in near 'specular' reflection that results in much smaller phase changes between elements.

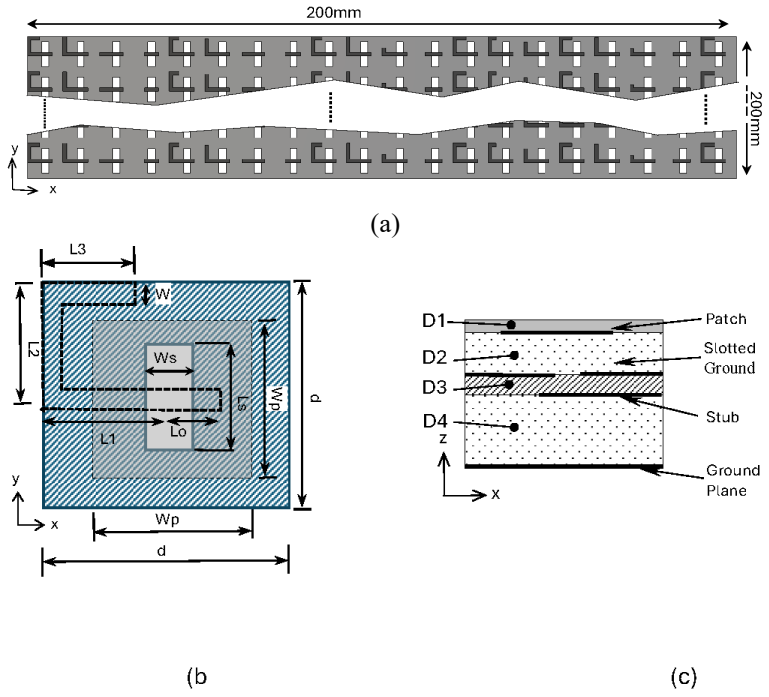

Figure 6. Details of prototype RAS (**a**) Overall view; (**b**) Details of element (from [18]): P = 10 mm, Wp = 7.5 mm, Lo = 2.0 mm, Ls = 7.0 mm, Ws = 2.0 mm, W = 1.0 mm; (**c**) Profile of structure: dielectric D1: 0.125 mm GTS550 (ε_r = 2.8, tanδ = 0.008); dielectric D2: 1.0 mm Rohacell 51HF Foam (ε_r = 1.067, tanδ = 0.0041); dielectric D3: 0.762 mm Neltek NY9250 (ε_r = 2.50, tanδ = 0.0015); dielectric D4: 5.0 mm Rohacell 51HF Foam

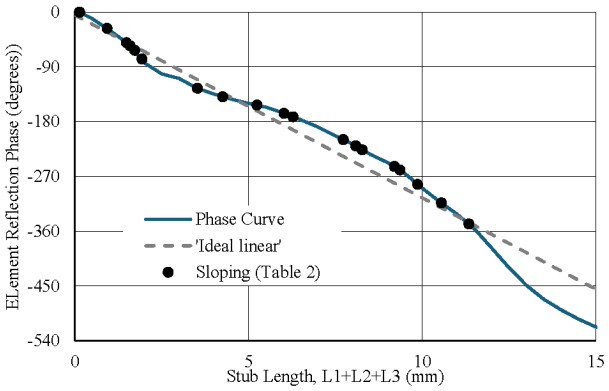

Figure 7. Element phase curve

Two RAS were fabricated, with one phased to give a flat-topped pattern around θo = 40° (i.e., Figure 3) and the second a sloped top pattern around Δθ = 40° (i.e., Figure 5). Details of the element stub lengths are recorded in Table 2

with the set of phases required for the sloping design also overlaid in Figure 7 for illustration. To calculate the element lengths the spline function in MATLAB is used to model the curve in Figure 7 that can then determine the element lengths for the wanted element phases. The RAS were linearly polarized in the x-direction with beam steering in the XOZ plane (i.e., TM polarization). Numerical simulations using the bistatic RCS tool in the frequency domain model of CST MWS were made for the practical designs and are presented in Figure 8 at three frequencies, 9.5 GHz, 10 GHz and 10.5 GHz (i.e., centre frequency ±5%). The flat-topped beam is close to the desired template, although the pattern falls away at higher angles. This is due to element factor [1] that can is more pronounced above 45°. The beam is reasonably insensitive to frequency but displays some frequency scanning as reported by [16]. The sloping beam is perhaps a little less affected by element factor but does exhibit much greater pattern deterioration at 9.5 GHz, so has limited bandwidth.

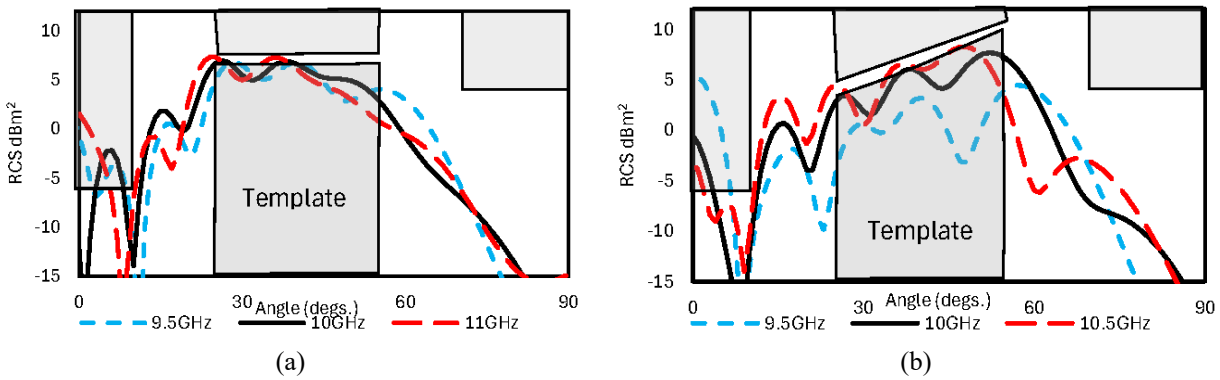

Figure 8. Simulations from CST MWS for prototype designs at different frequencies (**a**) Flat-topped beam (**b**) Sloping beam

Table 2. Element lengths for prototype designs

Element	Flat topped		Sloping	
	ψ_i	Ls_i	ψ_i	Ls_i
1	−41.5°	1.29	0.0°	0.13
2	−60.0°	1.68	−50.0°	1.48
3	−101.2°	2.47	−125.2°	3.52
4	−138.7°	4.24	−209.3°	7.73
5	−206.6°	7.63	−166.3°	6.02
6	−251.7°	9.15	−226.1°	8.28
7	−310.6°	10.49	−282.9°	9.87
8	−8.5°	0.42	−0.1°	0.13
9	−64.7°	1.76	−77.0°	1.93
10	−138.7°	4.24	−152.8°	5.24
11	−218.7°	8.06	−253.5°	9.20
12	−289.7°	10.01	−347.9°	11.35
13	−27.2°	0.94	−62.7°	1.72
14	−110.5°	3.08	−139.0°	4.26
15	−196.3°	7.26	−219.6°	8.09
16	−296.5°	10.16	−313.4°	10.56
17	−39.3°	1.24	−55.3°	1.59
18	−145.3°	4.66	−172.0°	6.28
19	−233.2°	8.49	−259.2°	9.36
20	−20.1°	0.75	−26.7°	0.92

The test arrangement used is illustrated in Figure 9. The RSR is held on a plastic (low-RCS) holder at a distance of 2.2 m from the transmit and receive horns, to meet the $2D^2/\lambda$ criteria. 10 dB standard gain horns were used to give an acceptable signal to noise ratio (~30 dB) but to reduce any phase variation across the RSR, i.e., to create a plane wave. The transmit horn was fixed on a stand at 2.2 m normal to the RSR. The receive horn was mounted on a stand fixed to a 2.2 m boom to allow rotation around the RSR. Measurement was made in an open plan laboratory but advantage was made of the time gating facility of the VNA to reduce the impact of unwanted reflections.

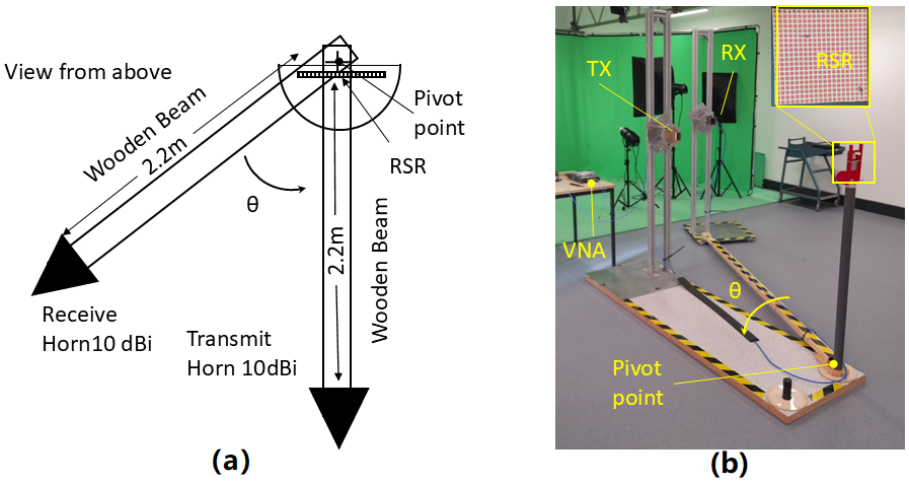

Figure 9. RSR Measurement arrangement (**a**) Schematic view from above (**b**) Photo of set-up

The bistatic RCS measurements are compared in Figure 10 to both the array factor and numerical simulations from the frequency domain analyzer in CST MWS. Overall the prototypes achieve the desired flat-topped and sloping-topped beams. There is excellent agreement between the measurements and CST although there are notable differences when compared to the AF model. Firstly the measured pattern reduces at higher angles (>45°) again due to the element factor not accounted for in (1) and (3). The array factor model was altered to include an element factor term of cos(θ) [1] and this improves the agreement between the AF and measurement/CST particularly at the higher positive angles and accounting for the flat beam sloping down as angle increases. Results from this design are compared to similar patterns from the literature in Table 3. Previous work looked to produce a beam that reduces with increasing angle, whilst this work sought to increase the beam. This is more difficult to achieve, needing to put more energy at higher angles, and this may explain the larger differences seen between simulation and experiment, although overall a reasonable comparison is seen.

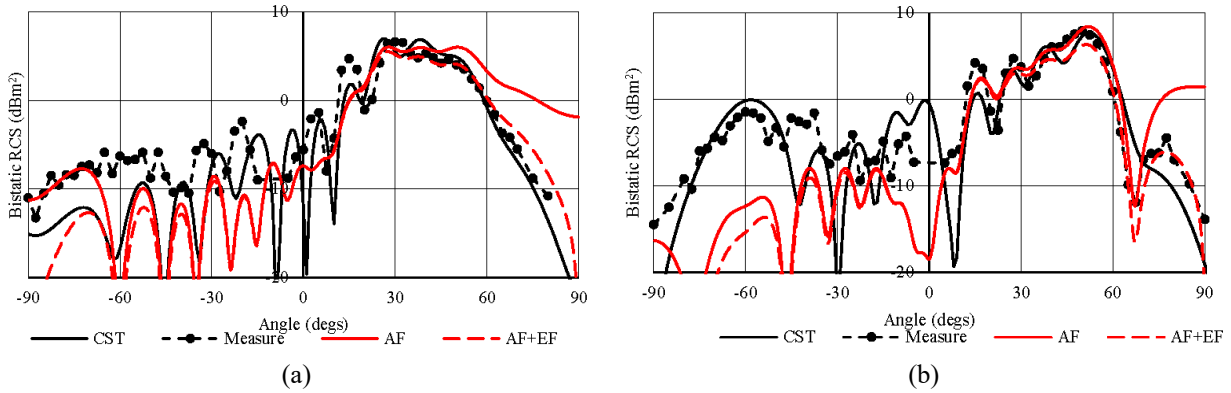

Figure 10. Measured bistatic RCS in XOZ plane for Ex (TM) illumination of array of Figure 5, with beam at $\theta_o = 40°$, $\Delta\theta = 30°$, with elements optimized for (**a**) flat-topped beam (as in Figure 2) (**b**) sloping beam (as in Figure 4)

There is increased 'ripple' in the wanted beams for CST/measurement not indicated by the array factor model. It is thought that this could be due to mutual coupling effects, detuning the element phases not accounted for in the AF model. In generating the curve of Figure 7 the element is modelled as being in an infinite array. However, it was noted for this design the phase step between elements is large, resulting in large physical differences between adjacent cells. This could lead to the actual element phase differing from that desired by the AF model. Referring back to Figure 2 the sloping topped

design also has a more complex phase distribution so would be more likely to be sensitive to element detuning effects. Further work will be to improve the AF model for closer agreement to CST for these designs.

Table 3. Comparison of reflectarray formed sloped beam patterns

Design	Frequency	N	Max beam angle	Beam shape	Variation of beam
[18]	10.4 GHz	25	30°	Slope decreasing with angle	Simulated ~3 dB Measured ~3 dB
[19]	25 Ghz	30	60°	Slope decreasing with angle	Simulated ~4 dB Measured ~6 dB
This work	10 GHz	20	55°	Slope increasing with angle	Simulated ~3 dB Measured ~7 dB

6. Conclusions

Shaped beam reflectarray surfaces have been considered that can provide a single solution to illumination of a shadow region in wireless communication systems. Flat-topped and sloping-top patterns for beams extending to 60° were considered. The array factor design approach was taken that is known to be reliable for reflectarray antennas but for the RSR designs considered here there were greater levels of inconsistency against the experimental results. However, simulations from CST MWS agreed well with experiment indicating that the array factor model is less reliable for RSR. Using a slope-topped pattern to compensate for range loss led to a more complex element phase distribution leading to increased pattern distortions and higher sidelobes. It may be such limitations can be overcome with better element choice and this is an area for further work. For practical applications the overall dimension of the shaped beam RAS would need to be much larger than it's linearly phased equivalent. In our example at 10 GHz this meant a factor of 5 requiring a 0.5 m side-length that may present manufacturing challenges for RAS at lower frequencies.

Conflict of interest

The authors declare no conflict of interest.

References

[1] P. Nayeri, F. Yang, and A. Z. Elsherbeni, *Reflectarray Antennas: Theory, Designs, and Applications*. Hoboken, NJ, USA: Wiley-IEEE Press, 2018. Online ISBN: 9781118846728.

[2] B. Kim, H. Kim, D. Choi, Y. Lee, W. Hong, and J. Park, "28 GHz propagation analysis for passive repeaters in NLOS channel environment," in *Proc. 9th Eur. Conf. Antennas Propag. (EuCAP)*, Lisbon, Apr. 13–17, 2015, pp. 1–4.

[3] L. Li, Q. Chen, Q. Yuan, K. Sawaya, T. Maruyama, T. Furuno, and S. Uebayash, "Novel Broadband Planar Reflectarray With Parasitic Dipoles for Wireless Communication Applications," *IEEE Antennas Wireless Propag. Lett.*, vol. 8, pp. 881–885, 2009.

[4] L. Li, Q. Chen, Q. W. Yuan, K. Sawaya, T. Maruyama, T. Furuno, et al., "Frequency selective reflectarray using crossed-dipole elements with square loops for wireless communication applications," *IEEE Trans. Antennas Propag.*, vol. 59, no. 1, pp. 89–99, 2011.

[5] Q. Chen, J. Li, Y. Kurihara, K. H. Chen, K. Sawaya, Q. Yuan, et al., "Experimental Investigation of Elimination Blindness Propagation Channel Using Reflectarray Parasitic Dipole," in *Proc. Int. Symp. Antennas Propag.*, Chicago, IL, USA, Jul. 8–14, 2012, pp. 1–2.

[6] D. Ha, D. Choi, H. Kim, J. Kum, J. Lee, and Y. Lee, "Passive repeater for removal of blind spot in NLOS path for 5G fixed wireless access (FWA) system," in *Proc. IEEE Int. Symp. Antennas Propag. & USNC/URSI Nat. Radio Sci. Meeting*, San Diego, CA, USA, Jul. 9–14, 2017, pp. 2049–2050.

[7] J. Li, Q. Chen, S. Qu, Q. Yuan, K. Sawaya, "Dual frequency reflectarray design using sandwiched FSS," in *Proc. Asia-Pacific Microw. Conf. (APMC)*, Yokohama, Japan, Dec. 7–10, 2010, pp. 877–880.

[8] P. Callaghan, P. Young, and C. Gu, "Corner reflectarray for indoor wireless applications," in *Proc. IET Antennas Propag. Conf.*, Birmingham, UK, Nov. 11–12, 2019, pp. 1–5.

[9] P. Callaghan, P. Giannakou, S. G. King, M. Shkunov, and P. R. Young, "Linearly Polarized Reconfigurable Reflectarray Surface," *IEEE Trans. Antennas Propag.*, vol. 69, no. 10, pp. 6480–6488, Oct. 2021, doi: 10.1109/TAP.2021.3070719.

[10] Metawave, "Businesswire," Accessed: Dec. 4, 2018. [Online]. Available: https://www.businesswire.com/news/home/20181204005253/en/NTTDOCOMO-Metawave-Announce-Successful-Demonstration-28GHz-Band.

[11] Editorial, "TMYTEK Unveils the XRifle Reflector Solution for Wider FR2 Extension and Effective 5G mmWave Coverage at Wireless Japan 2023," prnewswire.com. Accessed: May 25, 2023. [Online]. Available: https://www.prnewswire.com/news-releases/tmytek-unveils-the-xrifle-reflector-solution-for-wider-fr2-extension-and-effective-5g-mmwave-coverage-at-wireless-japan-2023-301834436.html.

[12] S. V. Hum and J. Perruisseau-Carrier, "Reconfigurable Reflectarrays and Array Lenses for Dynamic Antenna Beam Control: A Review," *IEEE Trans. Antennas Propag.*, vol. 62, no. 1, pp. 183–198, Jan. 2014, doi: 10.1109/TAP.2013.2287296.

[13] C. Pan, H. Ren, K. Wang, J. F. Kolb, M. Elkashlan, M. Chen, et al., "Reconfigurable intelligent surfaces for 6G systems: principles, applications, and research directions," *IEEE Commun. Mag.*, vol. 59, no. 6, pp. 14–20, 2021, pp. 14–20.

[14] B. Rana, S.-S. Cho, and I.-P. Hong, "Review Paper on Hardware of Reconfigurable Intelligent Surfaces," *IEEE Access*, vol. 11, pp. 29614–29634, 2023, doi: 10.1109/ACCESS.2023.3261547.

[15] R. Flamini, D. De Donno, J. Gambini, F. Giuppi, C. Mazzucco, A. Milani, "Towards a heterogeneous smart electromagnetic environment for millimeter-wave communications: An industrial viewpoint," *IEEE Trans. Antennas Propag.*, vol. 70, no. 10, pp. 8898–8910, Oct. 2022.

[16] C. A. Balanis, *Antenna Theory: Analysis and Design*, 3rd ed. Hoboken, NJ, USA: John Wiley & Sons, 2005, ISBN 0-471-66782-X.

[17] P. Callaghan and P. R. Young, "Beam- and Band-Width Broadening of Intelligent Reflecting Surfaces Using Elliptical Phase Distribution," *IEEE Trans. Antennas Propag.*, vol. 70, no. 10, pp. 8825–8832, Oct. 2022, doi: 10.1109/TAP.2022.3199451.

[18] O. M. Bucci, G. Franceschetti, G. Mazzarella, and G. Panariello, "Intersection approach to array pattern synthesis," *Proc. IEE H (Microw. Antennas Propag.)*, vol. 137, no. 6, pp. 349–357, 1990.

[19] H.-X. Xu, T. Cai, Y.-Q. Zhuang, Q. Peng, G.-M. Wang, and J.-G. Liang, "Dual-Mode Transmissive Metasurface and Its Applications in Multibeam Transmitarray," *IEEE Trans. Antennas Propag.*, vol. 65, no. 4, pp. 1797–1806, Apr. 2017, doi: 10.1109/TAP.2017.2673814.

[20] E. Carrasco, M. Arrebola, and J. A. Encinar, "Shaped Beam Reflectarray using Aperture-Coupled Delay Lines for LMDS Central Station," in *Proc. Sec. Euro. Conf. Antennas Propag. (EuCAP)*, Edinburgh, UK, Nov. 11–16, 2007, pp. 1–6, doi: 10.1049/ic.2007.1339.

[21] M. Arrebola, J. A. Encinar, and M. Barba, "Multifed Printed Reflectarray With Three Simultaneous Shaped Beams for LMDS Central Station Antenna," *IEEE Trans. Antennas Propag.*, vol. 56, no. 6, pp. 1518–1527, Jun. 2008, doi: 10.1109/TAP.2008.923360.

[22] V. Zuniga, A. T. Erdogan, and T. Arslan, "Adaptive radiation pattern optimization for antenna arrays by phase perturbations using particle swarm optimization," in *Proc. 2010 NASA/ESA Conf. Adaptive Hardw. Syst.*, Anaheim, CA, USA, Jun. 15–18, 2010, pp. 209–214.

[23] T. Ohsawa, T. Maruyama, M. Omiya, and N. Suematsu, "Design of Dual-frequency Reflectarray Using Particle Swarm Optimization," in *Proc. Int. Symp. Antennas Propag. (ISAP)*, Busan, Korea, Oct. 23–26, 2018.

[24] D. R. Prado, J. A. López-Fernández, M. Arrebola, M. R. Pino, and G. Goussetis, "General framework for the efficient optimization of reflectarray antennas for contoured beam space applications," *IEEE Access*, vol. 6, pp. 72,295–72,310, 2018.

[25] C. Capozzoli, C. Curcio, and A. Liseno, "Reflectarray synthesis on GPUs," in *Proc. 12th Euro. Conf. Antennas Propag. (EuCAP 2018)*, London, UK, Apr. 9–13, 2018, pp. 1–5, doi: 10.1049/cp.2018.0868.

[26] G. Oliveri, F. Zardi, P. Rocca, M. Salucci, and A. Massa, "Building a smart EM environment—AI-enhanced aperiodic micro-scale design of passive EM skins," *IEEE Trans. Antennas Propag.*, vol. 70, no. 10, pp. 8757–8770, Oct. 2022.